Available online at www.sciencedirect.com
SCIENCE DIRECT®
Thermochimica Acta 403 (2003) 65–81
thermochimica acta
www.elsevier.com/locate/tca

Integrated circuit thermopile as a new type of temperature modulated calorimeter

Mikhail Merzlyakov*

Department of Chemical Engineering, Texas Tech University, 6th and Canton, P.O. Box 43121, Lubbock, TX 79409-3121, USA

Received 20 November 2002; received in revised form 16 January 2003; accepted 31 January 2003

Abstract

Thermopiles, integrated into a thin silicon membrane, are used in some calorimetric applications (e.g. Setaram SETline120 portable thermal analyzer) that utilize temperature ramps of the thermostat to obtain the caloric response. A new calorimetric method is proposed, which uses an integrated circuit thermopile (ICT) in an oscillating mode. A heater integrated into the membrane drives temperature oscillations and the thermopile senses the temperature gradient across the membrane. ac calorimetry and the 3-omega method do not measure total heat losses and have an inherent quasi-adiabatic low frequency limit. On the other hand, the thermopile setup can measure total heat losses that permits one to monitor enthalpy changes in a sample, e.g. during crystallization. Low frequency measurements are limited only by sensor sensitivity. Preliminary results show that the same experimental setup can be used to make dynamic heat capacity measurements over a frequency range from 1 mHz to 100 Hz. At high frequencies (1 Hz and higher), heat capacity of nanogram samples can be measured.

Keywords: Temperature modulated calorimetry; Microcalorimetry; Nanocalorimetry; Dynamic heat capacity; Heat capacity spectroscopy

1. Introduction

Temperature modulated calorimeters (TMC) are widely used to measure complex (dynamic) heat capacity as a function of temperature, frequency and time providing unique information on relaxation phenomena (e.g. at glass transition and on melting and crystallization kinetics). Among traditional types of TMC, only temperature modulated differential scanning calorimeters (TMDSC) measure total enthalpy changes in a sample allowing study complex heat capacity as a function of the enthalpy. However, high frequency limit of TMDSC is rather low (0.1 Hz) compared to tens of Hertz in ac calorimetry and to 50 kHz in 3-omega method [1]. Alternative way to study relaxation phenomena as a function of the enthalpy is to perform time-domain analysis of the response of an adiabatic calorimeter, which makes it as an ultra low frequency spectrometer with high frequency limit in the order of 10 mHz [2]. The objective of the present work is to develop a temperature modulation technique, based on integrated circuit (IC) technology, for complex heat capacity measurements with appreciably higher frequency limit than that of TMDSC and with the capability of measuring total enthalpy changes. This modulation technique could be readily scaled down and would allow caloric measurements on small samples of sub-microgram weight and sub-micrometer thickness, complementary to thin film microcalorimeter [3] and high-speed scanning microcalorimetry [4].

* Tel.: +1-806-7420448; fax: +1-806-7423552.
E-mail address: mikhail.merzliakov@coe.ttu.edu (M. Merzlyakov).

0040-6031/03/$ – see front matter © 2003 Elsevier Science B.V. All rights reserved.
doi:10.1016/S0040-6031(03)00083-2

2. Physical basis

2.1. Dynamic heat capacity measurements using integrated circuit thermopile

One way of determining a heat flow rate is to measure the temperature gradient that the heat flow rate generates while passing through some thermal barrier. Thermopiles have some advantages compared to the other sensors, used for temperature difference measurement, such as a resistance bridge or a transistor pair: thermopile has an output without offset and offset drift and does not require any biasing. In addition to that, the Seebeck effect in silicon is rather large, 0.5–1 mV/K per junction [5], compared to typical 30–50 μV/K of standard metal thermocouples, and many junctions can be connected in series and be placed in compact sensor using integrated circuit technology. Such thermopiles, integrated into a thin silicon membrane, are already used in some calorimetric applications [6], which allow the heat flow rate measurements with detection limit in the order of 100 nW. Lerchner et al. [7] presented different possible constructions of integrated circuit (IC) calorimeters. Hoehne and Winter [8] studied transient response of an IC thermopile (ICT) sensor, from which one can theoretically obtain frequency dependent heat capacity data. However, to the best of my knowledge, nobody used ICT sensors in temperature oscillation mode and nobody presented dynamic heat capacity data from IC calorimeter.

Since some of ICT sensors have a heater integrated into the membrane, as shown in Fig. 1, to calibrate the gauge factor of the sensor, implementing temperature oscillations is possible by applying alternating current to the heater. Let us consider first which output signal one can expect from measuring an empty sensor in air by applying oscillating voltage with constant amplitude to the heater. At low frequency limit ($\omega \rightarrow 0$) at each moment of time, the sensor is in equilibrium and temperature gradient across the thermopile depends only on the power input. Therefore, the thermopile output should have constant, frequency independent amplitude and should be in phase with

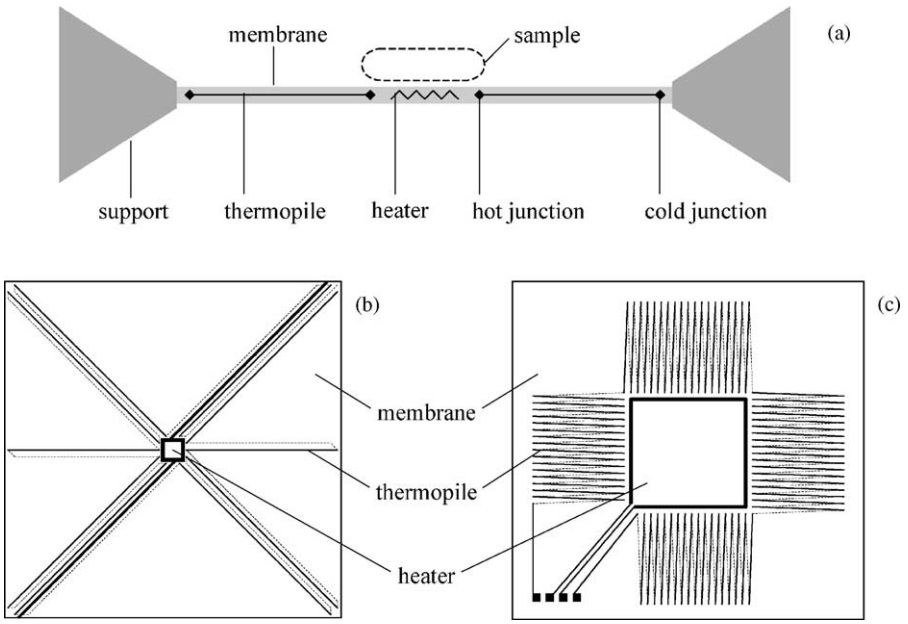

Fig. 1. (a) Schematic cross-section of ICT sensor (not to scale). Particular shape and proportions may vary. Sample under investigation can be placed on top of the membrane between the hot junctions. (b) Top view on ICT membrane with relative small heater and a few thermocouples, like in TCG-3875 sensor, see text below. (c) Top view on ICT membrane with relative large heater and a lot of thermocouples, like in LCM sensors, see text below.

the power input. At intermediate frequencies, part of the oscillating input power would be used to modulate the temperature of the membrane (heat capacity of the membrane becomes important). The rest of the oscillating power would result in smaller temperature gradient and, therefore, in smaller amplitude of the output signal. At high frequency limit ($\omega \to \infty$), temperature waves would not propagate far from the heater and would be already damped when reach to the hot junctions of the thermopile. This should result in much smaller amplitude of the thermopile output and in a large phase shift between the power oscillations and the output signal.

Relatively simple case for dynamic heat capacity measurements would be a situation when the frequency of temperature oscillations is low enough, so that the heater and the hot junctions of the thermopile oscillate in phase and with the same amplitude, yet the frequency is high enough, so that the temperature waves are damped completely at the cold junctions of the thermopile. This situation could be realized for a sensor with a small (relative to the membrane size) heater and hot junctions very close to it and with cold junctions far away from the heater, as shown in Fig. 1b. For some ICT sensors with relative large heater, as shown in Fig. 1c, this situation could never be realized. Denoting by HF_h the heat flow rate amplitude released on the heater and by T_h the temperature amplitude of the hot junctions at given frequency ω (with oscillating part of temperature equals to $T_h e^{i\omega t}$), we can write for empty sensor:

$$HF_h = i\omega T_h C_m \tag{1}$$

where C_m is the effective heat capacity of the membrane (including ambient gas parameters).[1] For the sensor loaded with a sample:

$$HF_h = i\omega T_h^* (C_m + C_{app}) \tag{2}$$

where C_{app} is the apparent heat capacity of the sample, described in Section 3. Since we keep HF_h constant by applying the same voltage amplitude to the heater U_{in}, T_h depends on the heat capacity of the sample. From Eqs. (1) and (2) we obtain

$$C_{app} = i\frac{HF_h}{\omega}\left(\frac{1}{T_h} - \frac{1}{T_h^*}\right) \tag{3}$$

The thermopile output voltage $U_{out}(t)$ is proportional to temperature difference between the hot and the cold junctions. Since cold junctions temperature stays constant, the amplitude of U_{out} becomes

$$U_{out} = \alpha T_h \tag{4}$$

where α is a calibration factor (real value), which is a Seebeck coefficient times the number of the thermocouples. Substituting Eq. (4) into Eq. (3), we have

$$C_{app} = i\alpha\frac{HF_h}{\omega}\left(\frac{1}{U_{out}} - \frac{1}{U_{out}^*}\right) \tag{5}$$

where U_{out} and U_{out}^* denote the thermopile output amplitude (complex value), measured for the empty and loaded sensor, respectively.

2.2. Apparent heat capacity

In general, apparent heat capacity value is measured instead of true value because of thermal lag (poor sample thermal conductivity, limited thermal contact conductance between a sample and a sensor, etc.). For example, if a small piece of metal is placed on the membrane, then apparent heat capacity C_{app} "seeing" by membrane in first approximation is given as [9]:[2]

$$C_{app}(\omega) = \frac{C_p}{1 + i\omega/K\,C_p} \tag{6}$$

where K is the value of thermal contact conductance between the sample and the membrane and C_p is the true heat capacity of the sample. The locus of C_{app} in polar plot is a semicircle, as shown in Fig. 2a, with a diameter equals to C_p. The lower the frequency or the higher the thermal contact conductance, the closer C_{app} is to C_p.

[1] All parameters in Eqs. (1) to (5) are complex and might be frequency dependent. Note that T_h is not necessarily proportional to $1/\omega$ and that the phase shift between HF_h and T_h does not equal to $\pi/2$ as it may appear. In this section particular frequency dependence of C_m is not of importance since the final Eq. (5) does not include C_m. Notation of frequency dependence, $f = f(\omega)$, is omitted for clarity.

[2] In [9], temperature oscillations were written as $T\exp(-i\omega t)$ resulting positive phase shift in case of response delay. Internal algorithm of the lock-in amplifier, used in experimental setup, operates with $\exp(i\omega t)$, resulting negative phase shift in delayed response. To keep the formalism the same throughout the paper $\exp(i\omega t)$ is used. Therefore, the conjugate value of C_{app} from reference [9] must be taken. The same is true for Eq. (7).

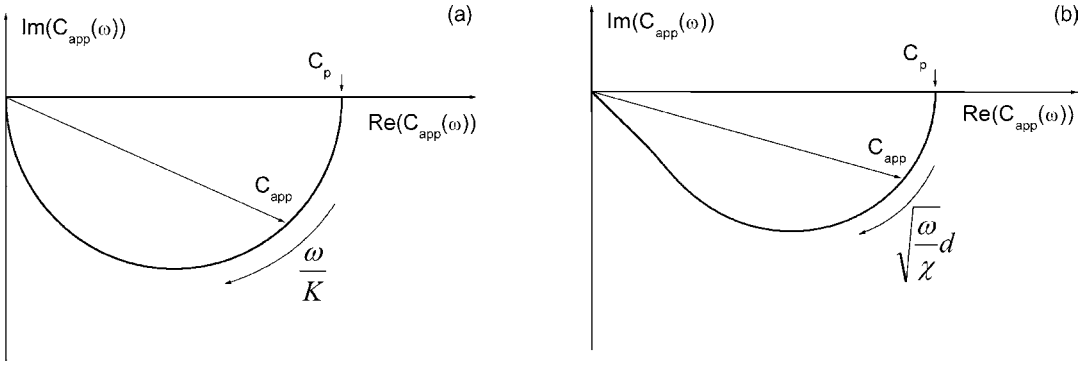

Fig. 2. Polar plots of an apparent heat capacity C_{app}, determined by: (a) a low thermal contact conductance between the sample and the membrane, (b) a poor thermal conductivity of the sample.

If a sample has a good adhesion with a membrane resulting nice thermal contact conductance, but poor thermal conductivity, as in polymers, then C_{app} in first approximation is given as [9]:

$$C_{app}(\omega) = \frac{1}{i\omega}\kappa S k \tanh(kd) \quad (7)$$

where κ is the sample thermal conductivity, S the sample contact area with the membrane, $k = \sqrt{-i\omega/\chi}$, $\chi = \kappa/\rho C_p$ the thermal diffusivity, ρ the sample density, c_p the sample specific heat capacity and d is the sample thickness. The locus of that C_{app} in polar plot is shown in Fig. 2b (parameter k may have two values opposite in sign, but they result the same unique value of C_{app}). The lower the frequency or the higher the sample thermal conductivity, the closer C_{app} is to C_p. In addition, C_{app} is closer to C_p when the sample thickness d is smaller. In real measurements, C_{app} can have influence of both a low thermal contact conductance and a poor thermal conductivity, and can be given by even more complicated expressions.

3. Experimental

Three types of ICT sensors were used: LCM-2524, LCM-2506 and TCG-3875 (Xensor Integration, The Netherlands). Details in the sensors design and manufacture can be found in [6]. For the measurements, each sensor was placed in a small temperature controlled aluminum box with one opening for equilibration of pressure and gas composition with surrounding air. A computer operated lock-in amplifier DSP-7265 (PerkinElmer Instruments, USA) was used to run an experiment. The output of the lock-in oscillator was directly connected to the sensor heater and the output of the thermopile was connected to the differential input of the lock-in. Unless otherwise stated, dc coupling mode was used to allow measuring offset value of the input voltage in addition to the amplitude and the phase angle. Input voltage after amplification ("monitor" output of the lock-in) was connected to the auxiliary integrating analog-to-digital converter of the lock-in, which measured the dc component of the voltage. Note that in spite the offset-less output from the thermopile (no heat flow rate—no signal) one has dc component in oscillation mode because of the offset of the periodic heat flow rate released in the heater. The lock-in readings of voltage amplitude are in root-mean-square amplitudes (rms amplitudes, $U_{rms} = A/\sqrt{2}$ for $A\sin\omega t$ or $Ae^{i\omega t}$). Later in the text, all voltage amplitudes (U_{in} and U_{out}) are given as rms amplitudes.

Aluminum and two polymer materials were used for the measurements: polystyrene (PS) obtained from Arco Polymers (PS-Dylene 8, $M_w = 221{,}000$ g/mol) and polycaprolactone (PCL) obtained from Aldrich Chemie ($M_w = 55{,}700$ g/mol).

4. Results

4.1. Frequency response behavior

Thermopile output signal for empty sensors is shown in Fig. 3. The results are as expected: at low

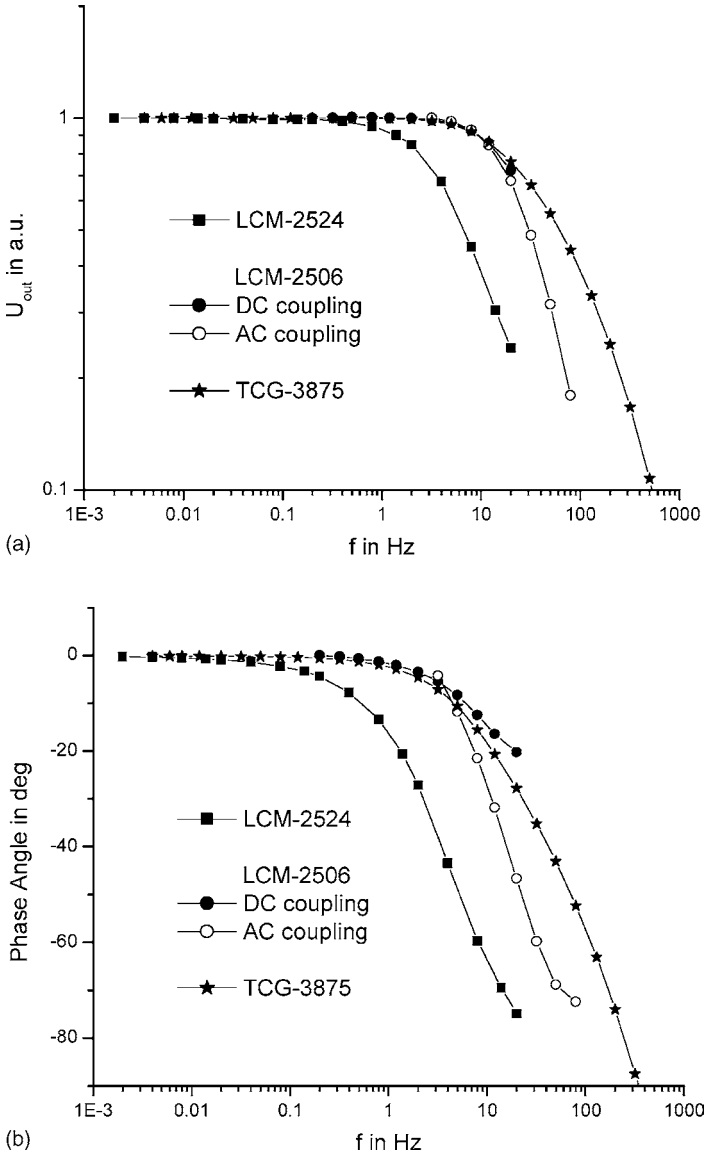

Fig. 3. Amplitude (a) and phase angle (b) of the output signal U_{out} vs. frequency of temperature oscillations for different sensors. The measurements of LCM-2506 were made in dc and ac coupling mode of the lock-in amplifier. The amplitude was normalized for better comparison since the sensors have different gauge factor.

frequencies the amplitude is constant and the phase angle is the same as that of power oscillations.[3] Deviation of the measured phase angle from 0° towards lower values at high frequencies corresponds to phase lag between the power oscillations and the thermopile output. LCM-2524 sensor, having the

[3] Note that lock-in amplifier measures phase angle relative to the oscillator voltage. If this voltage oscillates as sin ωt, then the power, released on the heater, oscillates as $\sin^2\omega t = (1 - \cos 2\omega t)/2$, i.e. on the second harmonic with the phase shift of 90° relative to the oscillator. This phase shift is subtracted from measured U_{out} values and HF_h in Eq. (5) is considered as a real (not a complex) number.

largest membrane (8.5 mm × 8.5 mm, 25 μm thick), shows the slowest response. LCM-2506 membrane is 3.5 mm × 3.5 mm and 8 μm thick. This sensor has a non-linear response at moderate input voltage, and output readings depend on coupling mode (see Section 5 for details). These two sensors are specially designed for caloric measurements. The third sensor (TCG-3875) is actually a vacuum gauge or thermal conductivity gauge and shows the fastest response. It has been initially designed to measure an effective thermal resistance between the sensitive area (silicon-nitride membrane) and the ambience (sensor support), which depends on the pressure and the type of the surrounding gas. By coincidence, it has the same construction (shown in Fig. 1) with membrane size of about 1.5 mm × 1.5 mm and 0.5 μm thickness, and can also be used for caloric measurements.

4.2. Linearity check

Test of linearity could prove whether or not a given ICT sensor is suitable to work in oscillating mode and gives a rough estimate of usable range of amplitude of power oscillations. In linear regime, the thermopile output voltage U_{out} at given frequency should be proportional to the input power, i.e. to square of input voltage applied to the heater U_{in}. The phase angle should be independent on U_{in}. Fig. 4 shows non-linear behavior of LCM-2506 sensor at moderate U_{in}. Output amplitude, as well as phase angle, depends on the coupling mode. ac coupling mode results in better linearity, but cannot be used to measure total heat flow rate and at frequencies lower than 1 Hz (because the input is connected via capacitance). As can be seen in Fig. 4 at frequency of 10 Hz and at low U_{in}, ac coupling mode affects the phase angle readings compared to dc coupling mode; however, there is no detectable changes in amplitude. The reason for the non-linearity of that sensor is unknown. There may be some parasitic coupling between the heater and the thermopile. To get reasonable measurements on that sensor one should apply voltage oscillations U_{in} not higher than 0.1 V.

TCG-3875 sensor shows substantially better linearity, as shown in Fig. 5, deviating only at the highest tested amplitude, $U_{in} = 3$ V. Different gain factors of the lock-in preamplifier may result slightly different values of phase angle as reflected by a small step in phase angle at $U_{in} = 3$ mV. Usage of low amplitudes is limited by the signal-to-noise ratio, which inevitably decreases with decreasing U_{in}. More detailed data of high amplitude response are shown in Fig. 6. Deviation from straight line starts at U_{in} higher than 1 V, regardless of voltage frequency.

4.3. Noise level

Noise affects the accuracy of measurements of thermopile output voltage U_{out}, as can be seen in Fig. 5 on the phase angle and amplitude of U_{out} for the two lowest values of U_{in}. As the voltage amplitude on the heater U_{in} increases, so does the U_{out} and noise can become below the detection limit of the main AD converter of the lock-in amplifier, as shown in Fig. 7. Long-term drift in U_{out} is determined by stability of temperature, of ambient gas composition and of U_{in} amplitude.

4.4. Apparent heat capacity measurements

Apparent heat capacity, calculated by Eq. (5), is shown in Fig. 8 for the measurements of PS droplet and aluminum foil pieces of different sizes on LCM-2506 sensor. At low frequencies measured C_{app} of aluminum reminds semicircles, as discussed in Section 2.2. Because of poor thermal conductivity, C_{app} of PS deviates much more from semicircle and reminds partly the shape of C_{app} curve in Fig. 2b. At high frequencies systematic deviations are appreciable. Some calibration is needed because LCM-2506 sensor has relatively large heater and the assumptions, made in derivation of Eq. (5), are not valid.

ICT sensors are relatively complicated systems to model their response to temperature oscillations. Another approach was used to empirically calibrate frequency response behavior of the sensors by applying calibration algorithm, described in [9,10]. Corrected apparent heat capacity of an aluminum disk (0.782 mg) after such calibration is shown in Fig. 9 for LCM-2524 sensor. This sensor has the largest membrane and would need the largest correction. The measured C_{app} agrees fairly well with theoretical values. For the calibration, a second aluminum disk ($m = 1.252$ mg, $K = 0.9$ mW/K) was used and specific heat capacity of aluminum was assumed to be 1 J/gK.

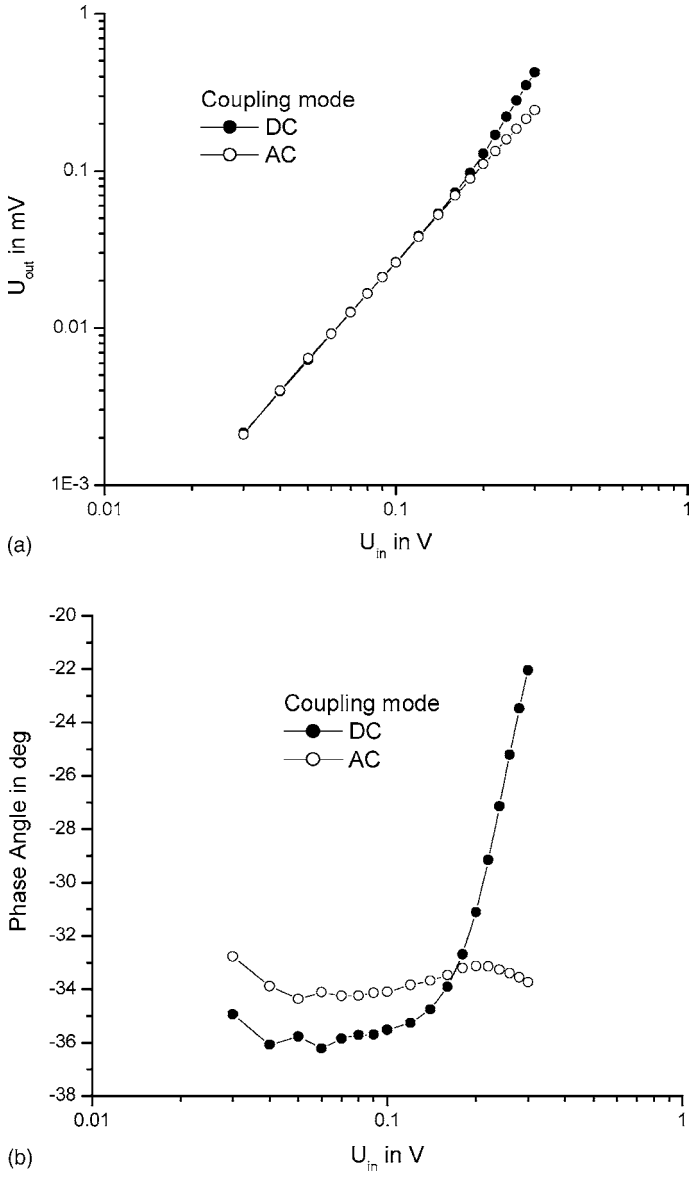

Fig. 4. Amplitude (a) and phase angle (b) of the thermopile output signal, U_{out}, vs. amplitude of the heater voltage, U_{in}, at dc and ac coupling mode. LCM-2506 sensor at 50 °C, oscillator frequency 10 Hz.

Knowing the correct value of C_{app} allows determination of true heat capacity of a sample, C_p. In case of a low thermal contact conductance, C_p equals to the diameter of a semicircle in polar plot representation of C_{app} and can be determined as $C_p = |C_{app}|/\cos(\mathrm{Arg}(C_{app}))$, where $\mathrm{Arg}(C_{app})$ is an argument (phase angle) of complex C_{app}. If a sample heat capacity is complex, C_p value can be calculated from C_{app} as describe in [11]. Note that in ICT measurement, one should set to zero heat capacity of sample pan if the sample was measured directly on the membrane.

Smaller and thinner membrane of the vacuum gauge is closer to the ideal simple situation, assumed in

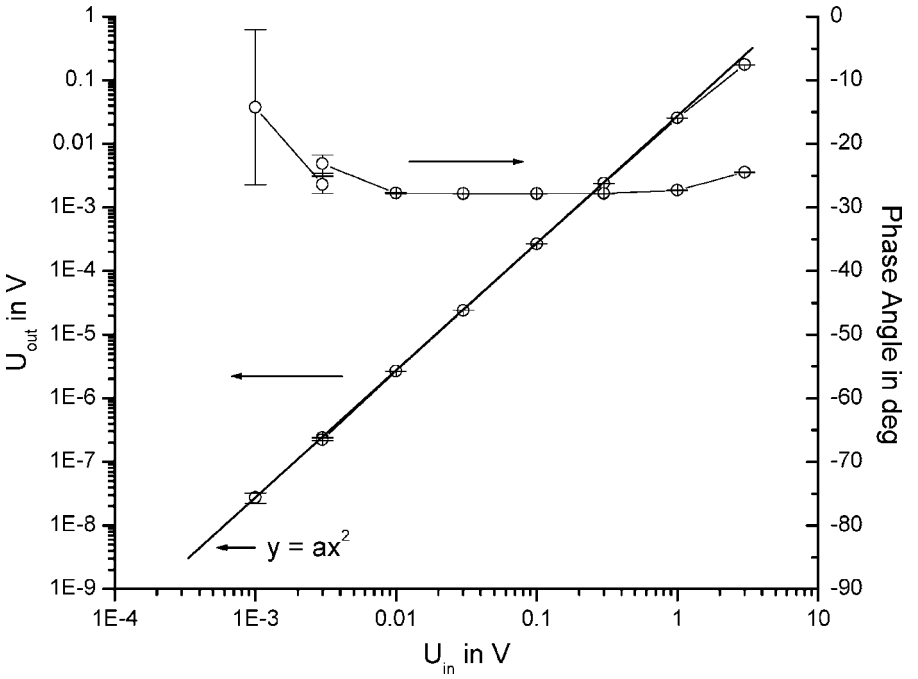

Fig. 5. Amplitude of the thermopile output voltage, U_{out}, and phase angle vs. amplitude of the heater voltage, U_{in}, at 10 Hz of oscillator frequency. TCG-3875 sensor at 50 °C.

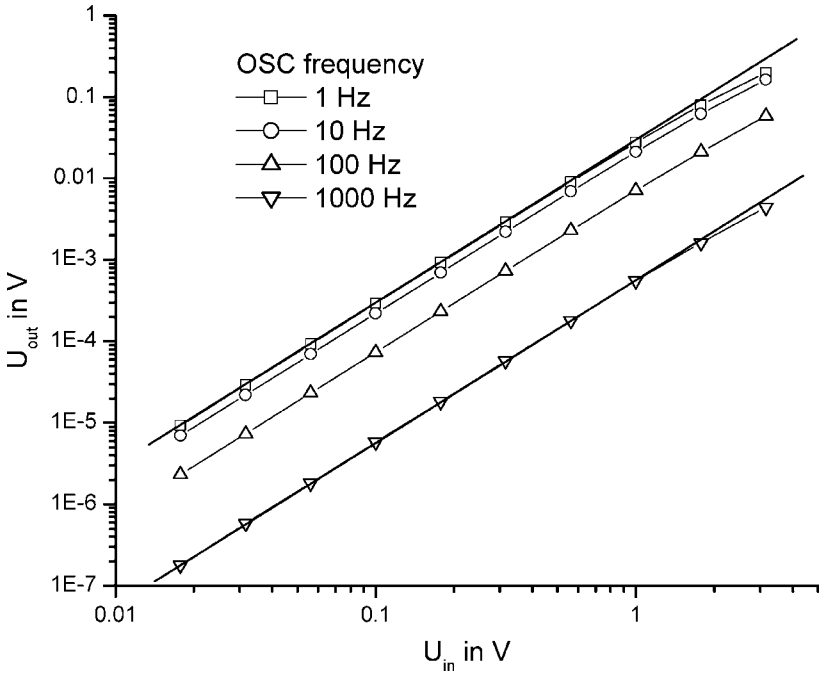

Fig. 6. Amplitude of thermopile output voltage, U_{out}, vs. amplitude of heater voltage, U_{in}, at different oscillator frequencies. TCG-3875 sensor at 50 °C. Error bars are much smaller than symbols size.

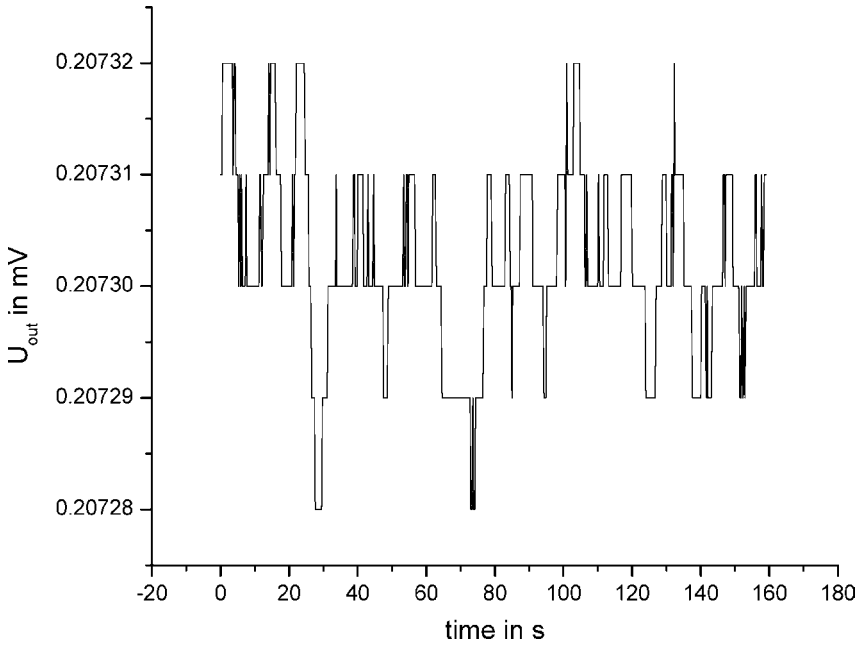

Fig. 7. Amplitude of thermopile output voltage U_{out} vs. time. TCG-3875 sensor at 50 °C, amplitude of heater voltage $U_{in} = 100$ mV, oscillator frequency 10 Hz, the lock-in time constant 1 s.

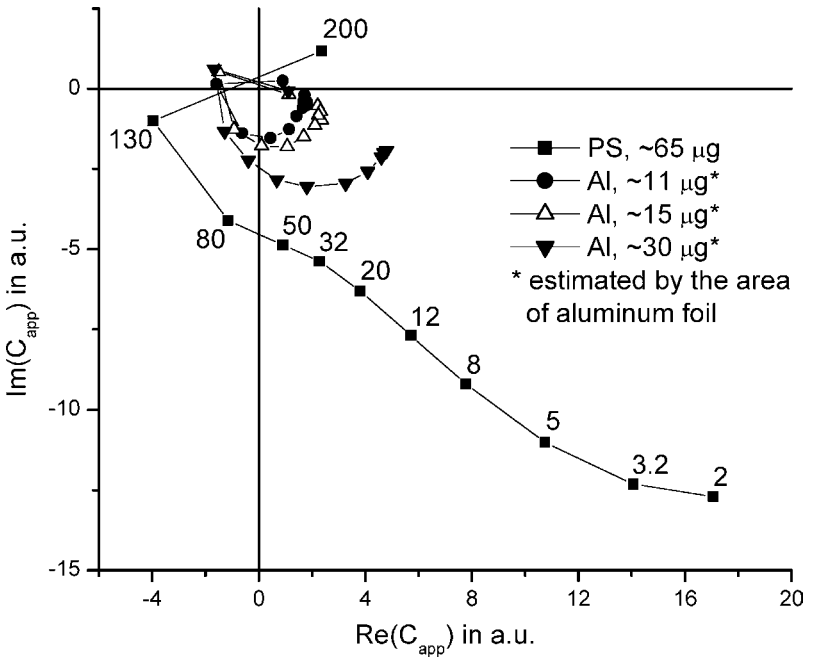

Fig. 8. Polar plot of apparent heat capacity C_{app} of different samples. C_{app} measured by LCM-2506 sensor at 40 °C. Numbers stand for the frequency of temperature oscillations in Hz.

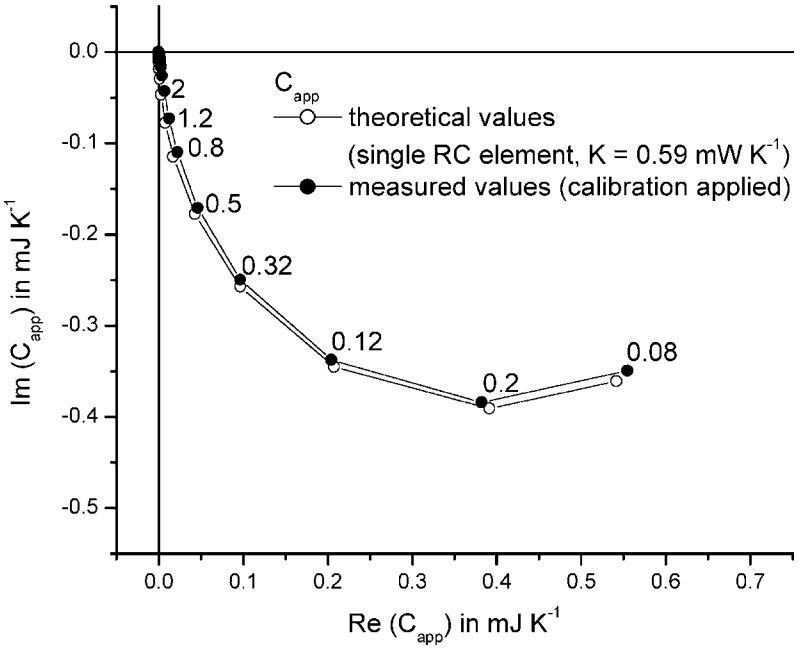

Fig. 9. Polar plots of apparent heat capacity C_{app} after dynamic calibration. LCM-2524 sensor at room temperature. Numbers stand for the frequency of temperature oscillations in Hz.

derivation of Eq. (5), mainly because the heater is very small and the hot junctions are much closer to the center of the membrane, than in other sensors, as shown in Fig. 1b. A very small droplet of dilute PCL solution in toluene was placed in the middle of TCG-3875 membrane and dried out. The changes in U_{out} are shown in Fig. 10. After the measurement, PCL was removed from the membrane by carefully rinsing it in toluene.

It may appear suspicious that phase angle curves of empty and loaded sensor cross each other and that above 20 Hz loaded sensor looks "faster" (the effect is even more pronounce in Fig. 14b). This can be explained by considering the steps of C_{app} calculation by Eq. (5). First, let us take U_{out} at around 20 Hz (Fig. 11a). Next, take reciprocal values (Fig. 11b). Finally, multiplication by $i\alpha HF_h/\omega$ brings the vectors $(1/U_{out} - 1)/(U^*_{out})$ into fourth quadrant, as expected for C_{app} (Fig. 11c). These steps can be followed backward and then it becomes plausible that at some particular C_{app} and U_{out} the phase angle of output of loaded sensor would be larger than that of empty sensor.

Apparent heat capacity of PCL sample, calculated by Eq. (5), is shown in Fig. 12. The value for α was set to 2.5 mV/K (see Section 4.6). From the value of heat capacity, the mass of the sample can be estimated to be in the order of 140 ng. The correction is needed at frequencies lower than 12 Hz (when probably the temperature of the cold junctions starts to oscillate) and at frequencies higher than 80 Hz (when a phase lag may exist between temperature oscillations of the heater and of the hot junctions). Theoretically, one can perform measurements at frequencies up to 2 kHz and still can see the difference between the empty and the loaded sensor. In that measurement, the droplet was accidentally placed half way out of the heater, which may account for low value of effective thermal contact K (see Eq. (6)) which leads to decrease in the modulus of C_{app} at relative low frequencies for that small sample.

4.5. Heat capacity of PS

A droplet of 5% PS solution in toluene was placed in the middle of TCG-3875 membrane. The droplet was much larger than that in Section 4.4. Then the sensor was kept above 100 °C for 1 day to evaporate

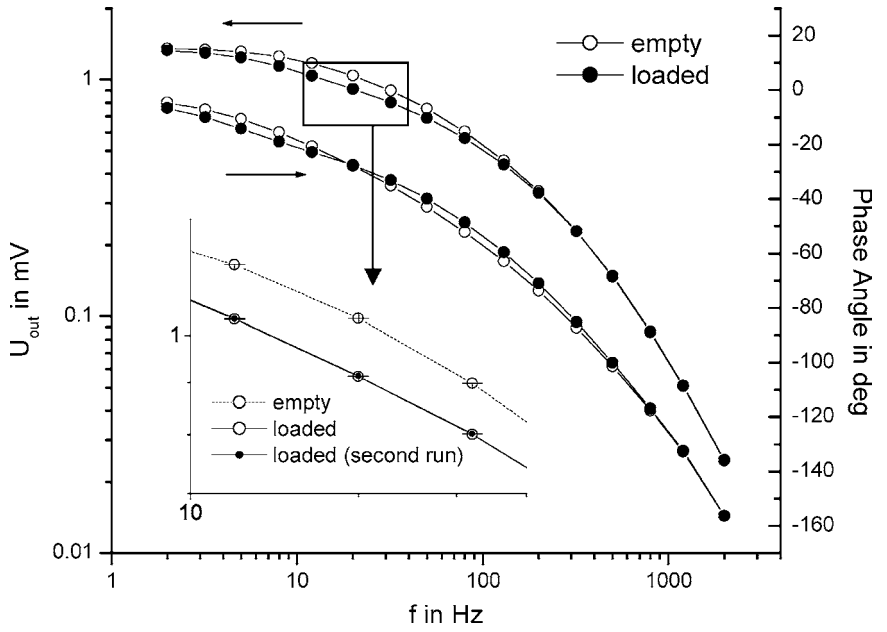

Fig. 10. Amplitude and phase angle of the thermopile output signal U_{out} vs. frequency of temperature oscillations for empty sensor and sensor, loaded with dried out droplet of PCL solution in toluene. TCG-3875 sensor at 50 °C.

residual toluene. After that, U_{out} was recorded under scanning of temperature with 1 K/min heating rate and C_{app} was calculated by Eq. (5). No further corrections were applied. The results are shown in Fig. 13. One can nicely see a step in modulus of C_{app} in glass transition region, as well as, negative peak in argument of C_{app} (phase angle). Note that C_{app} does not equal to the true sample heat capacity but distorted by thermal lag, which result an offset in phase angle and smaller step in the modulus of C_{app}.

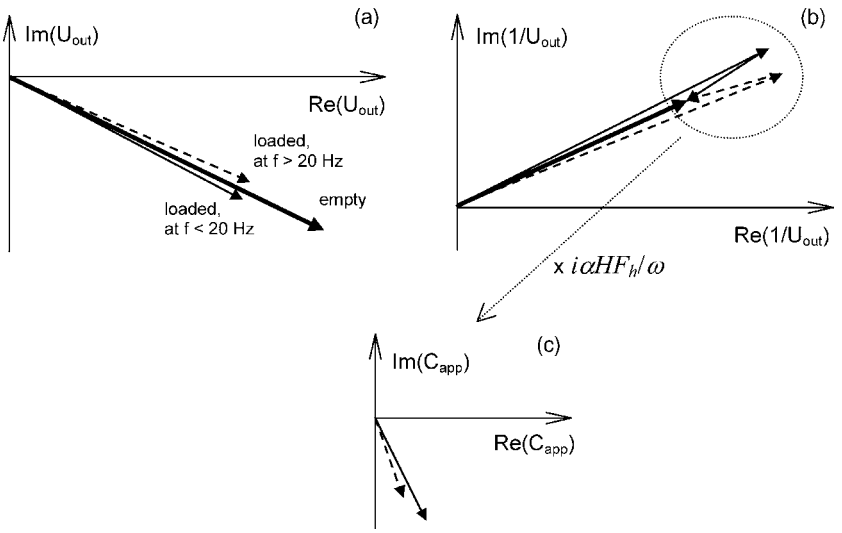

Fig. 11. Schematic representation of calculation steps of C_{app} by Eq. (5). The values of U_{out} were taken form Fig. 10 at around 20 Hz.

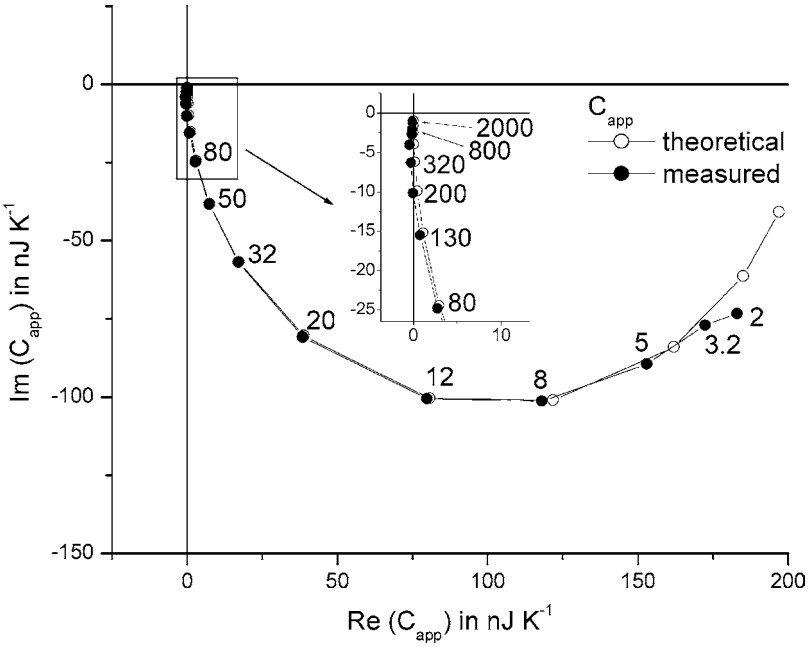

Fig. 12. Polar plot of apparent heat capacity of poly(caprolactone) (PCL). TCG-3875 sensor at 50 °C. Numbers stand for the frequency of temperature oscillations in Hz.

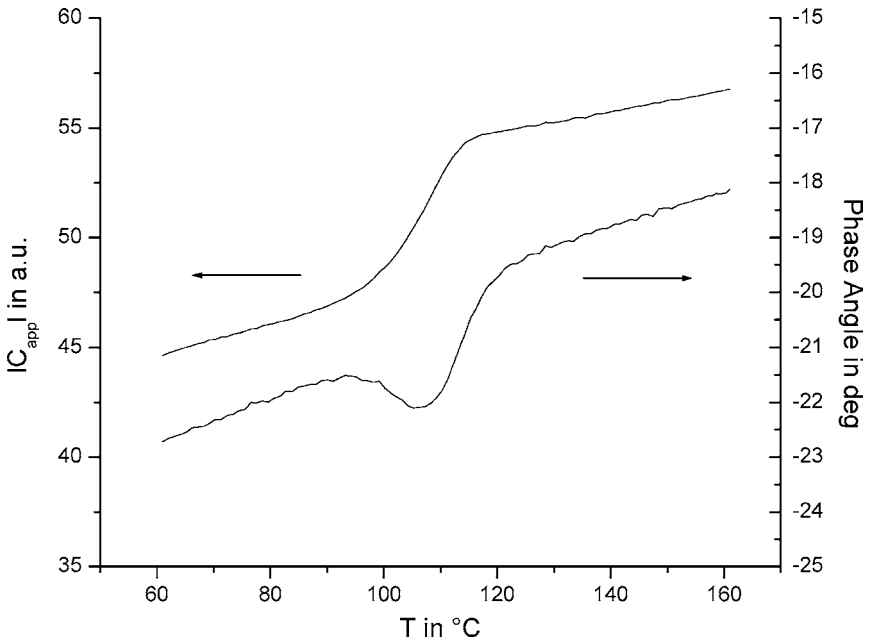

Fig. 13. Modulus and phase angle of apparent heat capacity of PS vs. temperature at 4 Hz of temperature oscillations. TCG-3875 sensor, underlying heating rate 1 K/min, 0.1 V oscillating amplitude on heater.

4.6. Thermopile calibration

Calibration of the gauge factor of ICT sensor (how it converts a heat flow rate into the voltage output) is relatively straightforward by using integrated heater. To get heat capacity scale, on the other hand, one needs to know calibration factor α in Eqs. (4) and (5). One way to determine this parameter is to measure a

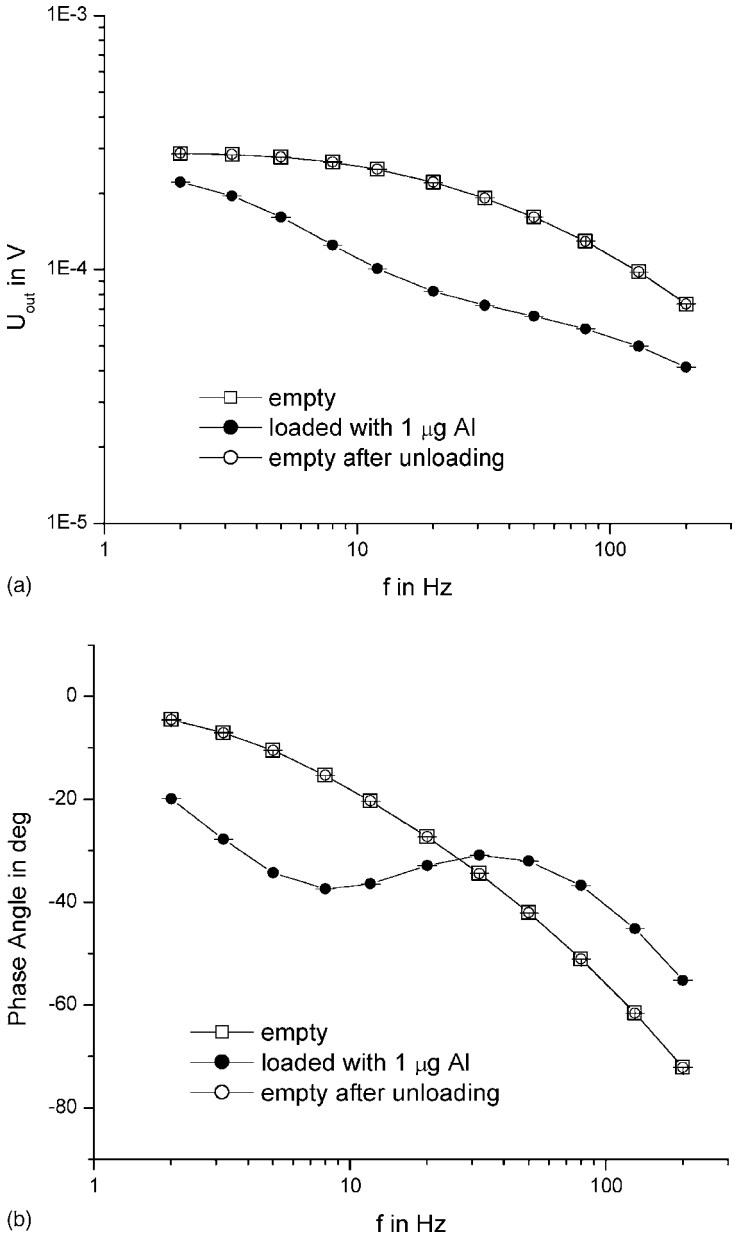

Fig. 14. Amplitude (a) and phase angle (b) of the output signal vs. frequency of temperature oscillations for three measurements of: (i) empty sensor; (ii) sensor loaded with 1 μg aluminum; and (iii) empty sensor after removing the sample. TCG-3875 sensor at 40 °C, $U_{in} = 100$ mV, error bars are smaller than symbols size.

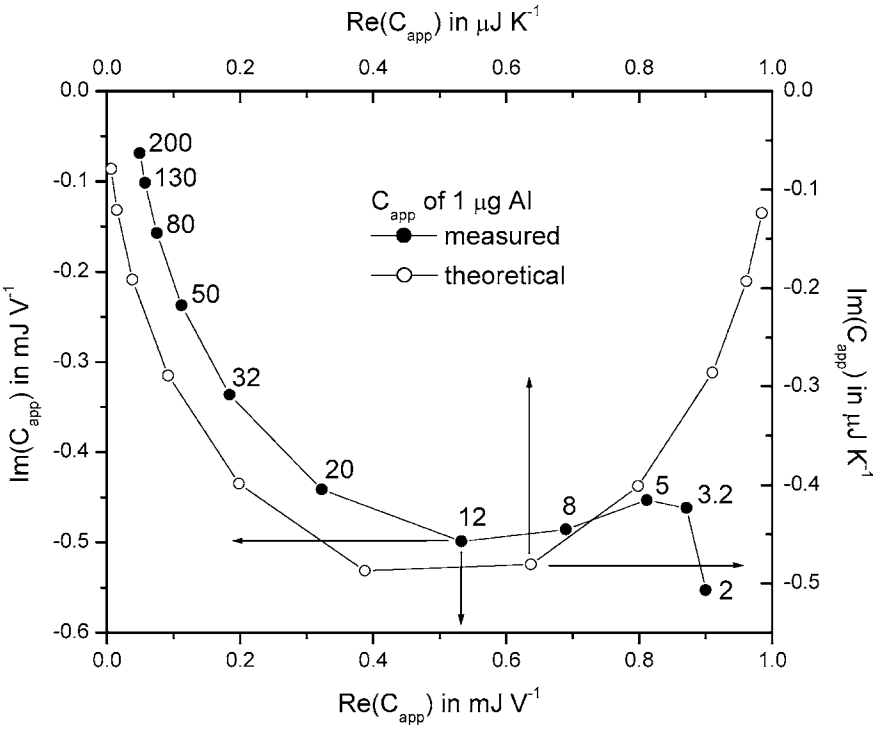

Fig. 15. Polar plot of apparent heat capacity of about 1 μg aluminum. Left and bottom axes represent measured C_{app} values, calculated by Eq. (5) by setting the calibration factor α to unit. Right and top axes represent theoretical C_{app} values, calculated by Eq. (6). TCG-3875 sensor at 50 °C. Numbers stand for the frequency of temperature oscillations in Hz.

sample with known heat capacity. Result of calibration of large ICT sensor (LCM-2524) is already shown in Fig. 9. ICT sensor on much smaller and thinner membrane of vacuum gauge (TCG-3875) is more sensitive to thermal load; therefore, much smaller samples are needed for calibration. Fig. 14 shows how amplitude and phase angle of U_{out} are changed by loading just 1 μg of aluminum.[4]

The presence of 1 μg piece of aluminum appreciably reduces U_{out} amplitude and affects the phase angle. Without knowing the calibration factor α in Eq. (5), one actually calculates heat capacity in J/V units. That C_{app} values are shown in Fig. 15 as bold points. On the other hand, sample mass and specific heat capacity of aluminum are known; therefore, expected C_{app} values can be plotted as well in right units (J/K) as shown in Fig. 15, open points. At frequencies lower than 8 Hz, cold junctions may start to oscillate; therefore, C_{app} calculated by Eq. (5) requires further calibration. This is consistent with the results in Fig. 12 where measured C_{app} at frequencies lower than 8 Hz deviates the same way from the expected semicircle. At high frequencies, some systematic deviation of measured C_{app} from the semicircle may be caused by dry inhomogeneous thermal contact conductance K between the sample and the membrane, which would have additional frequency dependence.

Matching both scales in the Fig. 15 results in an approximate determination of calibration factor as $\alpha = 1$ mV/K. Xensor Integration specified α for TCG-3875 to be equal to 2–2.5 mV/K. Exact α is necessary for

[4] Actual mass of that aluminum sample could differ by a factor of 2 since the author did not have access to sensitive enough balance. A mass of much large piece of aluminum foil was determined to be 60–70 μg , after that a 1/64 part of it was cut out and used for the measurement. Sample mass was the major source of error in α determination.

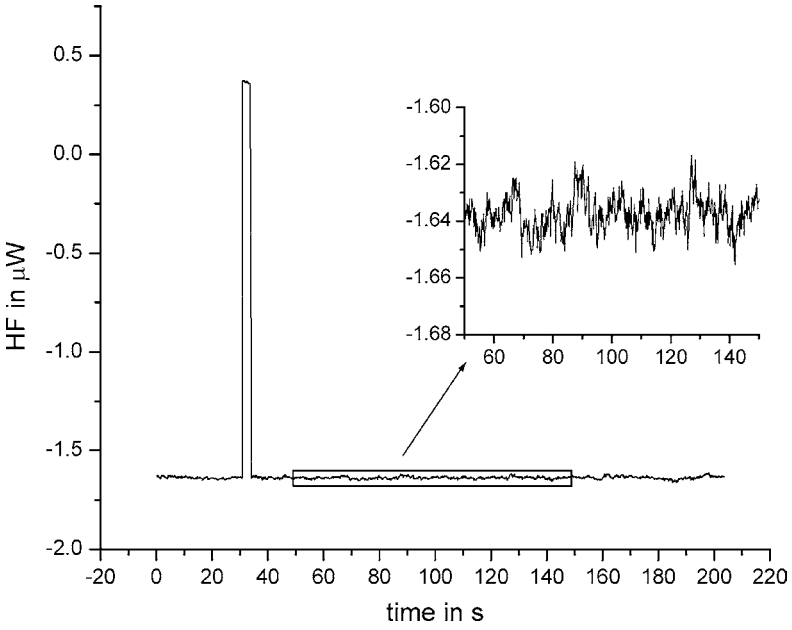

Fig. 16. Total heat flow rate with calibration pulse of 2 μW vs. time. TCG-3875 sensor at 50 °C, oscillator frequency 10 Hz, integrating time 100 ms.

correct determination of C_{app}. Since experimental determination of α had significant uncertainties, $\alpha = 2.5$ mV/K was used for further calculations.

4.7. Total heat flow rate calibration

Along with complex heat capacity measurements, based on oscillating part of the total heat flow rate, ICT allows to measure simultaneously an average value of the heat flow rate into or out of a sample. Although the presence of a sample on the membrane can change the overall heat transfer outside of the sensor, the gauge factor can be calibrated in situ by the integrated heater. The capability of measuring heat effects by LCM sensors is documented in [6,7]. Calibration of the heat flow rate scale of the vacuum gauge TCG-3875 is shown in Fig. 16. The calibration was done by changing the oscillator amplitude from 20 to 40 mV and back to 20 mV. Since the resistance of the heater was 610 Ω, the power changed for about 2 μW. Averaging of the thermopile output voltage was performed by integrating AD converter of the lock-in over 100 ms, which corresponds to two periods in heat flow rate oscillations.

5. Discussions

Commercially available ICT sensors provide relatively broad frequency range from 1 mHz up to 100 Hz and higher for temperature modulated calorimetry. Note that these sensors were not designed for optimum frequency response performance. The construction of the membrane, optimized for faster response, might have hot junctions just beneath or on top of the heater and the heater itself can be uniform planar geometry, instead of frame-like shape. TCG-3875 sensor has a little advantage in response time relative to LCM-2506 (see Fig. 3) because of slightly smaller lateral size, but it has much higher sensitivity because the membrane is much thinner. Sensitivity can be further improved by scaling down the sensor size and membrane thickness. From the performance point of view, it is more interesting to discuss the smallest available sensor.

For the vacuum gauge sensor, the main heat transfer is carried through the gas rather than through the membrane itself. Although thermopile senses only temperature gradient across the membrane, this gradient directly related to the heat losses via gas, allowing

correct heat flow rate measurements. TCG-3875 shows a very large, at least 6 orders of magnitude, dynamic range of periodic heat flow rate measurements, as can be seen from Fig. 5. At the very high heater voltage (3 V), the output is lower than expected. The reason for lowering the amplitude of U_{out} is the overheating of the center of the membrane. At higher temperatures, the resistance of the heater becomes higher resulting lower power release than expected. In addition, thermal conductivity of surrounding gas is increased, improving thermal coupling between heater and the surrounding. Therefore, at the same input power the amplitude of temperature oscillations decreases, resulting in lower thermopile output. Changing the Seebeck coefficient and increasing the membrane heat capacity may further affect the system response at high U_{in}. At $U_{in} = 3$ V and at 1 Hz of voltage oscillations, U_{out} equals to 0.2 V, which corresponds to 113 K of temperature amplitude (assuming $\alpha = 2.5$ mV/K and remembering that U_{out} is rms amplitude value). As can be seen from Fig. 3a, at 2 Hz of power oscillations U_{out} of TCG-3875 sensor almost reached saturated value, which means that the temperature already oscillated between ambient and some maximum value. Since the amplitude of temperature oscillation equals to 113 K, average heater temperature is 113 K above ambient temperature. At 100 Hz of voltage oscillations and at $U_{in} = 3$ V U_{out} equals to 60 mV, which corresponds to 34 K of temperature amplitude. To be able to realize such a large temperature oscillations at 200 Hz, the center of the membrane has to be heated up and cooled down with the heating rate amplitude of about 43,000 K/s so that the maximum cooling rate at least equals to 43,000 K/s. That high cooling rate is possible because of very low thermal inertia of the thin membrane and of the cooling medium that is 0.5 mm air gap between the membrane and the heat sink of the sensor. Narrowing this gap or using helium as purge gas may easily increase further the maximum cooling rate, but also may degrade the heat flow rate sensitivity.

Gauge factor of TCG-3875 sensor at ambient air is about 22.75 V/W. The uncertainties in the measurement of thermopile voltage amplitude δU_{out} can be below 20 nV, as shown in Fig. 7. This means that uncertainties in determination of the heat flow rate amplitude δHF are below 0.8 nW. At the same time, U_{out} equals to 0.2 mV, which corresponds to the temperature amplitude in the order of 0.1 K. At 20 Hz of temperature oscillations heating rate amplitude A_q equals to 14 K/s. The resolution of heat capacity calculation can be estimated as $\delta C_p \approx \delta HF/A_q = 60$ pJ/K. Note that this resolution can be achieved at room temperatures in ambient air quasi-isothermally with relatively small temperature oscillation amplitude of 0.1 K.

As shown in Fig. 16, the total heat flow rate resolution by TCG-3875 is about 20 nW. Further smoothing the curve may improve the heat flow rate resolution, but may worsen the resolution in time. Resolution of the heat flow rate amplitude is much higher (about 0.5 nW) due to signal recovery principle of the lock-in algorithm. The same is true for other sensors: using temperature oscillations improves calorimetric resolution. Sample heat capacity can be much smaller than that of the membrane. For example, 11 μg piece of aluminum is smaller and thinner than the membrane of LCM-2506 sensor, but can be accurately measured, as shown in Fig. 8. Dried out PCL droplet of 140 ng (Fig. 12) had lateral size of about 0.2 mm × 0.2 mm and, therefore, was about 4 μm thick. This is larger than the membrane thickness of the vacuum gauge, but as the insert in Fig. 10 suggests, the sensor is capable to resolve easily much smaller thermal load, i.e. much thinner samples can be measured. The repeatability is not an issue because the second run results the same U_{out} values within experimental uncertainties, which are much smaller than symbols size in the scale of Fig. 10.

The membrane of TCG-3875 sensor is very vulnerable. However, if a care is exercised, then loading and unloading a sample will not irreversibly change the membrane. As one can see from Fig. 14, after removing the sample, membrane shows exactly the same response as before loading, indicating good reproducibility.

The calibration of sensor frequency response allows extending low and high limits of the frequency range where Eq. (5) is valid. For example, at 0.08 Hz of temperature oscillations the amplitude and the phase angle of U_{out} of LCM-2524 sensor almost reaches the low frequency limit values (see Fig. 3), but C_{app} after calibration is as expected (see Fig. 9).

In general, ICT method for complex heat capacity measurements is applicable for all tested sensors. Note that in spite the fact that the heater and the thermopile do not have radial symmetry and in spite of further complications in sensor geometry (different

thickness throughout a membrane, scratch protections, huge heat losses via ambient gas, etc.), it is possible to calibrate the frequency response behavior of any of these sensors and get out reasonable apparent heat capacity data at different frequencies of temperature oscillations. These data have the same importance as apparent heat capacity measured by TMDSC and can serve to calculate heat capacity spectrum, precise heat capacity or thermal conductivity (if the sample geometry is known).

ICT calorimeters offer the possibility of measuring samples with small lateral size (smaller than 0.2 mm) that is very important. It can minimize inhomogeneity of sample thickness, of local thermal contact with the membrane, of local heater resistance and can allow measuring not only thin films, but also micro samples like monocrystals.

6. Conclusions

A new type of temperature modulated calorimeter (ICT method) based on commercially available IC thermopile sensors is developed. The experimental setup is very simple consisting of the sensor, temperature controller and a lock-in amplifier. The method allows measurement of complex heat capacity together with total enthalpy changes of microgram-sized samples with high frequency limit of at least 100 Hz. Low frequency measurements are limited by sensor sensitivity. The resolution of the rate of enthalpy changes is in the order of 20 nW at 100 ms averaging time. Resolution of dynamic heat capacity can be as low as 60 pJ/K at room temperature in ambient air. This resolution can be achieved by quasi-isothermal measurements with temperature oscillation amplitude of 0.1 K. Dedicated sensors can improve resolution and increase high frequency limit.

Acknowledgements

The work was initially started at Rostock University, Germany. I would like to sincerely acknowledge Professor Christoph Schick, Rostock University, who introduced me to this field. I acknowledge Professor G. Wolf, Technical University–Bergakademie Freiberg, for introducing to the concept of integrated circuit calorimetry and Professor Gregory B. McKenna, Texas Tech University, for support. Thanks to Sander van Herwaarden, Xensor Integration, for providing valuable information about the sensors.

References

[1] Y.H. Jeong, Thermochim. Acta 377 (2001) 1–7.
[2] H. Suga, Thermochim. Acta 377 (2001) 35–49.
[3] D.W. Denlinger, E.N. Abarra, K. Allen, P.W. Rooney, M.T. Messer, S.K. Watson, F. Hellman, Rev. Sci. Instrum. 65 (1994) 946–959.
[4] S.L. Lai, G. Ramanath, L.H. Allen, P. Infante, Z. Ma, Appl. Phys. Lett. 67 (1995) 1229–1231.
[5] A.W. van Herwaarden, P.M. Sarro, Sens. Actuators A 10 (1986) 321–346.
[6] A.W. van Herwaarden, P.M. Sarro, J.W. Gardner, P. Bataillard, Sens. Actuators A 43 (1994) 24–30.
[7] J. Lerchner, A. Wolf, G. Wolf, J. Therm. Anal. Calorimet. 57 (1999) 241–251.
[8] G.W.H. Hoehne, W. Winter, Chip-calorimeter for small samples, in: Poster Presented at 17th IUPAC Conference on Chemical Thermodynamics; Book of Abstracts, 2002, pp. 273–274.
[9] M. Merzlyakov, C. Schick, Thermochim. Acta 330 (1999) 65–73.
[10] G.W.H. Hoehne, M. Merzlyakov, C. Schick, Thermochim. Acta 391 (2002) 51–67.
[11] M. Merzlyakov, G.W.H. Hoehne, C. Schick, Thermochim. Acta 391 (2002) 69–80.